

Response to Editors comments

All edits have been incorporated.

Reference to meristem in figure to has been changed to epithallus and change has been made in the figure.

Figure 5- vertical axis line has been changed to black and thickened, labels are already on this axis.

1 ANATOMICAL STRUCTURE OVERRIDES TEMPERATURE CONTROLS ON
2 MAGNESIUM UPTAKE - CALCIFICATION IN THE ARCTIC/SUBARCTIC
3 CORALLINE ALGAE *LEPTOPHYTUM LAEVE* AND *KVALEYA EPILAEVE*
4 (RHODOPHYTA; CORALLINALES)

5 Merinda C. Nash

6 Walter Adey

7 Department of Botany, National Museum of Natural History, Smithsonian Institution,
8 Washington, DC, USA, 20560

9

10 Author for correspondence: nashm@si.edu

11 Running title: Magnesium and anatomy in coralline algae

12 Key words: Coralline algae, calcification, biomineralization, magnesium, temperature,
13 proxy

14

15

16 Abstract

17

18 Calcified coralline red algae are ecologically key organisms in photic benthic
19 environments. In recent decades they have become important climate proxies, especially
20 in the Arctic and Subarctic. It has been widely accepted that Magnesium content in
21 coralline tissues is directly a function of ambient temperature, and this is a primary basis
22 for their value as a climate archive. In this paper we show for two genera of
23 Arctic/Subarctic corallines, *Leptophytum laeve* and *Kvaleya epilaeve*, that previously
24 unrecognized complex tissue and cell wall anatomy bears a variety of basal signatures for
25 Mg content, with the accepted temperature relationship being secondary. The
26 interfilament carbonate has lower Mg than adjacent cell walls and the hypothallial cell
27 walls have the highest Mg content. The internal structure of the hypothallial cell walls
28 can differ substantially from the perithallial radial cell wall structure. Using high-
29 magnification Scanning Electron Microscopy and etching we expose the nm-scale
30 structures within the cell walls and interfilament. Fibrils concentrate at the internal and
31 external edges of the cell walls. Fibrils ~10 nm thick appear to thread through the radial
32 Mg-calcite grains and form concentric bands within the cell wall. This banding may
33 control Mg distribution within the cell. Similar fibril banding is present in the
34 hypothallial cell walls but not the interfilament. Climate archiving with corallines can
35 achieve greater precision with recognition of these parameters.

36 **Introduction**

Rob Nash 9/11/17 11:46 AM

Deleted: This paper is part of a series of investigations on controls on Mg uptake and distribution within the crusts of a range of coralline genera.

41 Understanding tissue complexity and the structural organization of cell wall calcification
42 in coralline algae is important for many reasons, including the growing use of these
43 organisms as climate proxies and concern for the ecological effects of ocean acidification.
44 There is a burgeoning interest in using coralline crusts as environmental proxies for late
45 Holocene temperature (Hetzinger et al. 2009, Gamboa et al. 2010, Halfar et al. 2010),
46 arctic ice sheet coverage (Halfar et al. 2013) and pH changes with time (Krayesky-Self et
47 al. 2016). Typically magnesium content is used as a key indicator of late Holocene
48 temperature fluctuations (Adey et al. 2013). Yet despite this utilization of coralline
49 carbonate crusts for proxy climate research, there has been little study of tissue and
50 cellular-scale physiology as it relates to the distribution of magnesium within the crust.
51 Nor are the basic mechanisms of calcification fully understood (Adey 1998). This is in
52 stark contrast to the status of other calcifiers used for proxy work, e.g. corals (Barnes and
53 Lough 1993), foraminifera (Bentov and Erez 2005) and bivalves (Wanamaker et al. 2008).
54 However, these well-known climate proxies have little application in the Arctic Region
55 of greatest climate change affects (Adey et al. 2013), and without a greater understanding
56 of coralline calcification physiology, precision proxy analysis of temperature and other
57 environmental conditions, using coralline algae, is limited.

58

59 One of the key roles of corallines is the building of carbonate substrate that underpins
60 many ecosystems globally. For example, the thick bioherms found in coral reef
61 structures (Adey 1978a, b, 1998), the extensive rhodolith beds off South American
62 (Amado-Filho et al. 2012, Bahia et al. 2010) and Australian (Harvey et al. 2016) shores,
63 maerl substrate in the Mediterranean (Martin et al. 2014) and the dominant rocky benthos

64 biostromes and rhodoliths in many Arctic and Subarctic environments (Adey et al. 2013).
65 There are concerns that as atmospheric $p\text{CO}_2$ increases and consequent ocean
66 acidification increases, there will be negative impacts on the capacity of corallines to
67 continue building these important substrates (e.g. McCoy and Kamenos 2014), [although](#)
68 [there are experimental studies that find no negative impacts \(e.g. Cox et al., 2017\)](#). The
69 pace of research on the effects of temperature and climate change on coralline algae has
70 outpaced both the published data on anatomy and our understanding of the biochemical
71 processes controlling their carbonate skeletal building. For developing reliable past
72 climate proxy information using corallines and anticipating future climate change impacts
73 on these keystone calcifiers, as with any other organism, it is first necessary to understand
74 how these algae organize their tissues, build their skeleton and control cellular-scale
75 magnesium content.

76
77 While numerous studies of coralline growth rates under a wide range of temperature and
78 light conditions have been published (Adey and McKibben 1970, Adey 1970, 1973, Adey
79 and Vassar 1975, [Kamenos et al. 2008](#), [Diaz-Pulido et al. 2014](#), [Vásquez-Elizondo &](#)
80 [Enriquez 2016](#)), little attempt has been made to relate this information to calcification
81 processes. Also, it is only recently, with the use of higher magnification scanning electron
82 microscopy (SEM) (Adey et al. 2005, 2015a) that the earlier implications of anatomical
83 complexity (Adey 1964, 1965, 1966a, [Cabiocch and Giraud 1986](#)) have been fully
84 appreciated. It has been proposed that calcification is a result of locally elevated pH
85 during photosynthesis leading to super-saturation and associated mineral precipitation
86 (Ries 2010). However, some parasitic corallines lack photosynthetic pigments, and have

87 haustoria to derive nutrition from their hosts, yet present typical tissue and calcified wall
88 structures (Adey and Sperapani 1971, Adey et al.1974). Also, anatomical and magnesium
89 content studies of Arctic corallines demonstrate that growth continues in Arctic winter
90 darkness (Halfar et al. 2011, Adey et al. 2013), indicating that calcification is not likely a
91 straight forward association with micro-saturation state, as seen in some algae (e.g.,
92 *Halimeda*, Adey 1998, Sinutok et al. 2012).

Rob Nash 9/11/17 11:52 AM

Deleted: . There has been an experiment recording continued calcification at night and in the dark (experiment in progress)

93
94 Following on from the classical coralline studies, maturing around the turn of the 19th
95 century, Adey (1964, 1965,1966a,b) laid out the basic tissue-structured anatomy of
96 crustose corallines, adding the epithallium, intercalary meristem and cellular elongation
97 (while calcified) to the classical model of perithallium and hypothallium. Later, SEM
98 (Adey et al. 2005, Adey et al.2012) demonstrated greater sub-tissue complexity and
99 added the calcified cell wall components inner wall (IW) and interfilament (IF). It should
100 be noted that while the interfilament is a minor component of total calcification in the
101 species of this paper, it can be a major component in some genera (Adey et al. 2013,
102 2015a).

Rob Nash 9/11/17 11:54 AM

Moved down [1]: In this paper, we rename the inner wall the cell wall and retain the terminology interfilament, noting this is equivalent to the middle lamella in higher plants (Esau 1953); interfilament has also been referred to as interstitial (Ragazzola et al. 2016). We use the abbreviations PCW and PIF (perithallial cell wall and perithallial interfilament) and HCW and HIF (hypothallial cell wall and interfilament) to designate the carbonate wall components.

103
104 In this paper, we show for the first time the cellular-scale and anatomical controls on
105 magnesium distribution within the carbonate skeletons of two Arctic/Subarctic coralline
106 species. These are *Leptophytum leave* (Stromfelt) Adey, and the epiphytic (and non-
107 photosynthetic parasitic) *Kvaleya epilaeve* Adey and Sperapani, from the northern
108 Labrador Coast. *L. leave* is photosynthetic and forms expansive, but thin crusts (up to
109 one mm in thickness) generally on shell fragments and pebbles in deeper water (Adey

124 1966a, 1970). *K. epilaeve* is an epiphytic parasite, lacking in photosynthetic pigment, and
125 producing hypothallial haustoria that penetrate upper perithallial cells of *L. leave* (Adey
126 and Sperapani 1971). It is similar in physiology to the North Pacific Subarctic parasite
127 *Ezo epiyessoense* (Adey et al. 1974), which, along with its host *Lithophyllum yessoense*,
128 lies in a distantly related coralline group. *K. epilaeve* is the only known Arctic genus of
129 algae (Adey et al. 2008) and is absent or of very limited occurrence in Subarctic waters,
130 where the host continues to be abundant (Adey and Sperapani 1971). Understanding and
131 contrasting calcification within these two species, both growing in the same temperature,
132 light and pH conditions, offers an opportunity to examine the wide variance of Mg
133 content as a function of skeletal anatomy and metabolic processes.

134

135 **Methods**

136 *Sample collection and site information*

137 The sample was collected on 22nd July 2013, at the commencement of Arctic summer,
138 from 16-18 m depth at inner Port Manvers Bay, Labrador. The collection site lies at 56°
139 57.1' N; 61° 32.8' W., near the northern end of the 50 km long Port Manvers Run, a
140 north/south passageway inside of S. Aulatsivik Island (Fig. 1A, C). Sea ice is extensive
141 from November through early July, and the inter-island passages and bays are covered
142 with sea ice through much of that period. At the collection site, the bottom was a
143 shell/pebble gravel bed primarily of shell fragments and pebbles encrusted with *L. leave*,
144 *L. foecundum* and *Clathromorphum compactum*; scattered coarse rhodolith
145 *Lithothamnion glaciale* and *Lithothamnion tophiforme* were also present (Fig. 1B, D). *K.*
146 *epilaeve* occurred on *L. leave* and *L. leave* grew on both sides of the shell fragments.

Rob Nash 9/11/17 11:56 AM

Deleted: snow-covered land fast

148 | Salinity was 30 and measured using electronic induction instrumentation, November to
149 | July near surface water temperatures, below the sea ice, are within the -1.5 to -1.8° C
150 | range. Bottom summer temperature measured at the site on 22nd July 2013 was 0.5°C.
151 | Since this is relatively early in the summer season, peak temperatures are likely to be
152 | between 3-5°C (Adey et al. 2015) with a mean growing season temperature of ~ 2 ° C.
153 | This mean estimate is based on measurements from eight sites in the region (182 km S to
154 | 35 km N) with surface to bottom temperature records for 1964 (Adey 1966c) and 2013
155 | (Adey et al. 2015). These ranged from 1.9 to 5.6° C during summer at 15-20 m. The
156 | snow-covered land fast sea ice overlying the gravel rhodolith bed from which the samples
157 | were taken likely precludes significant solar energy from reaching the bottom for eight
158 | months of each year.

Rob Nash 9/11/17 11:56 AM

Deleted: and was 30 ppt

159 |
160 | The original sample is 2013-11(1) at the National Museum of Natural History.

Rob Nash 9/11/17 11:58 AM

Deleted: -

Rob Nash 9/11/17 11:58 AM

Deleted: Species identification was made by WHA.

161

162 **Analytical methods**

163 *Scanning electron microscopy- energy dispersive spectroscopy (SEM-EDS)*

164 | The CCA sample was fractured, mounted using carbon tape and platinum coated prior to
165 | scanning electron microscopy energy dispersive spectroscopy (SEM-EDS). For these
166 | analyses, we used a Zeiss UltraPlus field emission scanning electron microscope
167 | (FESEM) equipped with an HKL electron backscatter diffraction (EBSD) operated at 15
168 | kV, 11 mm working distance. SEM was carried out at the Australian National University
169 | Centre for Advanced Microscopy. SEM-EDS was used for spot analyses to quantify the
170 | elemental composition of representative parts of the CCA crust. A range of SEM settings

175 were used for imaging. The more common secondary (SE) electron showing topography,
176 backscatter electron imaging (BSE) which shows higher magnesium areas as darker
177 carbonate and is useful for rapid visual identification of mineral distribution.

178

179 A second round of EDS was undertaken using a NOVA NanoSEM FEI at the National
180 Museum of Natural History's Department of Mineralogy. Typically EDS measurements
181 are made using 15 kV (Nash et al. 2011) so that there is sufficient energy to dislodge
182 electrons from a range of elements, e.g. from lighter magnesium up to heavier strontium.

183 The EDS beam interacts with a roughly spherical-shaped region of carbonate beneath the
184 surface. This region is referred to as the interaction volume. At 15 kV the interaction
185 volume is ~ 3 µm in diameter whereas the average cell wall thickness ranges from only
186 500 nm up to ~2 µm (occasionally thicker, up to 3 µm). Interfilament in these species
187 may be only a few grains wide, 200-500 nm up to 2 µm. These narrow areas of interest
188 in contrast to the larger beam interaction volume, pose a problem for obtaining accurate
189 Mg measurements for only cell wall or interfilament. For example, a measurement of the
190 cell wall may include minor amounts of carbonate from the adjacent interfilament and
191 vice versa. Generally even with this beam crossover, in our experience 15 kV is sufficient
192 to identify a significant offset in magnesium while still collecting information that may
193 be of interest such as strontium levels. However, where there are only a few grains of
194 interfilament, as in the *L. leave*, the 3 µm interaction volume is problematic. A range of
195 EDS settings were tested aiming to reduce the beam interaction volume so that Mg
196 content for each the cell wall and the interfilament could be individually measured
197 without the beam crossing into the adjacent substrate. A setting of 7 kV, working distance

Rob Nash 9/11/17 11:58 AM

Deleted: enough

199 | 6.4 mm and 1 nA current was used to measure the interfilament grains in the *L. leave*
200 | with a count time of 20 seconds. The sample was carbon coated. This was calculated to
201 | have an interaction volume of <1 μm. These results are reported separately to the main
202 | data set.

203

204 *Sample preparation*

205 | Initially the crust was fractured using shears and mounted in superglue. After first
206 | imaging of the fractured crust, the sample was polished using 2000 gsm wet and dry
207 | sandpaper then sonic cleaned in unbuffered deionized water for 2 minutes. This
208 | preparation was used for SEM EDS measurements; 8-9 measurements were made for
209 | each carbonate type of interest. Subsequently the sample was sonic cleaned in unbuffered
210 | deionized water for 20 minutes. The deionized water has a pH of ~6.5. When cleaned
211 | for 2 minutes the surface is very lightly etched allowing differentiation between different
212 | Mg-calcite morphologies without altering the measured Mg content. After cleaning for
213 | 20 minutes there is a visible difference in the surface with much of the interfilament Mg-
214 | calcite and smaller grains removed allowing imaging of nm scale cellular structures.

215

216 X-ray diffraction methods

217 | Powder XRD was carried out using a SIEMENS D501 Bragg-Brentano diffractometer
218 | equipped with a graphite monochromator and scintillation detector, using CuKα radiation.
219 | A subsample was broken off the edge of the crust. This piece included *L. leave* with
220 | surficial *K. epilaeve*. The sample was ground using a mortar and pestle. Fluorite was
221 | added as an internal standard. The sample was not bleached and acetone was not added

222 during the grinding as this has been found to occasionally induce alteration and
223 precipitation of other minerals in other coralline samples we have worked with. Scan
224 interpretation for mol% MgCO₃ followed the methods described by Nash et al. (2013).

225
226 Terminology

227 In this paper, we rename the inner wall the cell wall and retain the terminology
228 interfilament, noting this is equivalent to the middle lamella in higher plants (Esau 1953);
229 interfilament has also been referred to as interstitial (Ragazzola et al. 2016). We use the
230 abbreviations PCW and PIF (perithallial cell wall and perithallial interfilament) and
231 HCW and HIF (hypothallial cell wall and interfilament) to designate the carbonate wall
232 components.

233

234 **Results**

235 *SEM imaging overview*

236 The specimen of *L. laeve* encased an aragonite carbonate shell. (Fig. 2A). The crust is
237 approximately 500 μm thick (Fig. 2B) with a basal hypothallus ~80 μms thick. *K.*
238 *epilaeve* has been considered to be an adelphoparasite, a species very closely related to its
239 host. Although diminutive, and superficially appearing as scattered white sand grains, *K.*
240 *epilaeve* can densely coat *L. laeve*. Although often appearing as densely crowded
241 conceptacles, it can possess the full basic array of anatomical features: hypothallium,
242 perithallium and epithallium (the latter mostly absent, Adey and Sperapani 1971) (Fig.
243 2B). *L. laeve* typically has an epithallium that is one cell layer of rounded ovoid, thin
244 walled cells that are often absent in SEM sections. The *K. epilaeve* grows directly on the
245 *L. laeve* meristem (Fig. 2C, D) and there was no evidence of excavation required (by

Rob Nash 9/11/17 12:01 PM
Deleted: [1]

Rob Nash 9/11/17 11:54 AM
Moved (insertion) [1]

Rob Nash 9/11/17 12:02 PM
Deleted: microns

Rob Nash 9/11/17 12:03 PM
Deleted: micron

250 borers or grazers), prior to settlement. This suggests that unlike the typical sloughing
251 relationship with epiphytes wherein epithallium builds up under the epiphyte until it
252 sloughs off, the *L. laeve* does not recognize *K. epilaeve* as foreign. The perithallial cell
253 walls of *L. laeve* contain radially-oriented grains of Mg-calcite; the interfilament is thin
254 and has carbonate grains randomly orientated in a plane parallel to the filament axis or
255 cell top/ bottom. The interfilament shows up strongly as stripes on vertical fracture
256 sections (Figs. 2B, C). Note for easiest viewing of the fine structures, the figure images
257 are best viewed on screen rather than in print.

258

259 The first layer formed by the *K. epilaeve* has angular grains parallel to the *L. laeve*
260 surface (Fig. 2E). The bottom part of the cell wall is without radial structure and has
261 submicron beads appearing to calcify along and within organic fibrils (Fig. 2E). Organic
262 fibrils are visible between the basal layer of *K. epilaeve* carbonate grains and the
263 meristem of the *L. laeve* (Fig. 2F) suggesting a method of attachment in addition to the
264 haustoria developed by some hypothallial cells (Adey and Sperapani 1971). There were
265 no haustoria visible in our SEM sample. Fine radial grains typically observed in cells of *L.*
266 *laeve* beneath the meristem were not apparent in the cell walls of the *L. laeve* meristem
267 (Fig. 2E,F) suggesting this surficial carbonate may have been altered or remineralised
268 during the attachment process.

269

270 *SEM-EDS*

271 Measurements for magnesium content in *Leptophytum laeve* were undertaken on both the
272 upper (side with conceptacles) and under (without conceptacles) crusts (Fig. 3A, D). The

273 | parasite, *Kvaleya epilaeve* was present on both surfaces (Fig. 2A, B Fig. 3A).
274 | Measurements of *K. epilaeve* were made on the underside.
275 |
276 | The Mg content of the perithallial and hypothallial cell walls of *L. laeve* was measured
277 | (Fig. 3 A-D) as well as what appeared to be a transitional cell type between the basal
278 | hypothallus and the typical perithallial cells (Fig. 2 D-F). These transitional cells are
279 | within the perithallus but have thin cell walls similar to the hypothallial cells. There are
280 | clear visual differences between the cell walls of the three cell types. The perithallial cell
281 | walls are 1-2 µms wide with clearly radial Mg-calcite (Fig. 2B, F). The basal
282 | hypothallial cells are elongated relative to the perithallial cells and their cell walls are
283 | narrower and do not always show radial cell wall structure (Fig. 2C). The transitional
284 | cells have elongate cells relative to the perithallus but less so than the hypothallus, and
285 | their cell walls are thinner, ~ 0.5 – 1 µm and do not show radial structures. The
286 | interfilament of *L. laeve* has only a single layer of Mg-calcite grains (Fig. 2B, F), as noted
287 | above showing as a thin line on longitudinal axial fractures; fractures along the
288 | interfilament appear as conspicuous vertical stripes (Figs. 2C).
289 |
290 | The *K. epilaeve* in the portion of the sample mounted for SEM did not present the typical
291 | elongated hypothallial cells as shown by Adey and Sperapani (1971), as this cut is not
292 | longitudinally placed on a growing lobe. The key difference between the perithallus of
293 | the *L. laeve* and *K. epilaeve* was the presence of wide (1-2 µms) areas of interfilament in
294 | the *K. epilaeve* (Fig. 3F, 4A, B). In many corallines (Adey et al. 2005), including the *L.*
295 | *laeve* studied for this paper there is only a single layer of interfilament grains, and these

Rob Nash 9/11/17 12:04 PM
Deleted: micron

Rob Nash 9/11/17 12:04 PM
Deleted: micron

Rob Nash 9/11/17 12:04 PM
Deleted: micron

299 | are present as vertical stripes on vertical fractures (Fig. 3B). EDS measurements were
300 | taken for both the *K. epilaeve* cell wall and interfilament (Fig. 4A, B). As the interaction
301 | volume of the EDS beam is ~ 3 µms (Methods) and the cell wall and interfilament
302 | thickness range from 1-3 µms, the values measured for both may include small amounts
303 | of the other, although every effort was made to place the beam on the widest part of the
304 | appropriate band. A second set of measurements was taken for the *L. leave* cell wall and
305 | interfilament using lower kV and the results are reported separately.

306

307 *Mg content*

308 Bulk whole sample content of Mg, determined by powder XRD was 10.8 mol% MgCO₃
309 (Mg/Ca 0.13). The EDS-determined average Mg content ranged from 9.1 (*K. epilaeve*
310 Perithallial interfilament) to 16.7 mol% MgCO₃ (*L. leave* upper Hypothallial cell wall),
311 (Table 1, Fig.6). The highest measured individual Mg content, 19.6 mol% MgCO₃, was
312 in the *L. leave* upper crust HCW. Generally the Mg content of interfilament was lower
313 than cell walls, and perithallial cell walls had the highest Mg content. The lowest values
314 were for the *K. epilaeve* PIF and PCW, 9.1 and 10.1 mol% MgCO₃ respectively, not
315 significantly different at significance level of 0.05 but are significantly different at
316 significance level of 0.1 (p= 0.068) (Table 2). Keeping in mind the values for the cell
317 wall and interfilament include a small amount of carbonate from the other, we consider
318 the p=0.068 result likely does represent a true significant difference between the two. The
319 PCW for the *L. laeve* was slightly higher at 11.2 and 12.9 mol% MgCO₃ (under and
320 upper crust respectively), these were not significantly different from each other (p=0.112).
321 The combined average of the upper and under *L. leave* cell walls (12.2 mol% MgCO₃)

Rob Nash 9/11/17 12:04 PM

Deleted: micron

Rob Nash 9/11/17 12:04 PM

Deleted: micron

324 was significantly higher ($p=0.025$) than the *K. epilaeve* cell wall. However, comparing
325 only the *L. laeve* cell wall of the under crust, the same side as the *K. epilaeve*, there was
326 no significant difference ($p=0.124$). The greatest difference between the upper and under
327 *L. laeve* crust was found between the hypothallial cell walls. The under HCW averaged
328 12.3 mol% $MgCO_3$, whereas the upper HCW was 4.4 mol% higher at 16.7 mol% $MgCO_3$.
329 The upper HCW was significantly higher than the *L. laeve* PCW's but not different from
330 the transitional CW's (15.6 mol% $MgCO_3$). Based on the graph in figure 5 this upper
331 range of Mg would equate to temperatures above $9.3^\circ C$, more than double the known
332 summertime highs at the sampling site.

333

334 The results for comparison of the cell wall and interfilament grains in the *L. laeve* using 7
335 kV showed the interfilament, 8.5 mol% $MgCO_3$ ($n=6$), was significantly lower ($p=0.001$)
336 than the cell wall, 11.1 mol% $MgCO_3$ ($n=8$).

337

338 **Structural features**

339 *Cell wall*

340 Within the radial Mg-calcite structure (PCW) of the *K. epilaeve*, a concentric banding
341 pattern is present (Fig. 7 A-C). The radial Mg-calcite grains are not always one
342 continuous long grain. The banding is aligned to the presence of organic fibrils that
343 appear regularly throughout the PCW (Fig. 7B). Organic fibrils, ~10 nm thick, are
344 parallel to the cell wall edges. These are spaced 30-40 nm apart throughout the middle of
345 the cell wall. It appears that the fibrils are mineralized. At the outer edges of the cell wall
346 the number of fibrils increases and appear as a dense mesh approaching a membrane (Fig.

347 7B, C) that is infilled with carbonate. The parallel fibrils are connected to the radial Mg-
348 calcite grains, appearing as if to continue through the grain (Fig. 7C), similar to fence
349 wire threading through fence posts at pre-defined spacing. There are also fibrils that
350 drape over the grains. Where the fibrils concentrate to a mesh, this is also calcified but
351 with smaller grains without regular shape. In the *K. epilaeve* interfilament (PIF), the
352 grains are aligned to the cell wall surface (Fig. 7C). Fibrils also run through the PIF and
353 attach to the interfilament grains but not with the regular pattern seen in the cell wall.
354 Looking at a cross section of the cell wall from the top down (Fig. 7D), the fibrils can be
355 seen to form a dense mesh.
356

357 Similar features are visible in the *L. laeve* PCW (Fig. 8A, B), although the organic fibrils
358 are not as well exposed. Possibly these cell wall grains are less susceptible to dissolution
359 in the etching treatment making it more difficult to expose the organic features. The
360 radial cell wall grains appear anchored to the external edge of the cell wall, immediately
361 adjacent the interfilament.

362

363 After etching for 20 minutes, more of the organic fibrils are exposed in the *K. epilaeve*
364 interfilament (Fig. 9A) revealing a porous membrane. PIF grains have angular edges in
365 contrast to the rounded sides of the cell wall grains. The *L. laeve* perithallial
366 interfilament has rice-grain shaped Mg-calcite flattened against the external side of the
367 cell wall (Fig. 9B) with attachment fibrils. Fibrils are visible stretching between the
368 flattened interfilament grains on adjacent cells (Fig. 9C).

369

370 Hypothallial cell walls at 200-500 nm wide are much thinner than perithallial cell walls
371 (Fig. 10 A-C). The HCW internal structure appears roughly radial (Fig. 10 A- C). But, the
372 radial structure is not always well developed with parts of the HCW exhibiting a distinct
373 break down the middle of the radial structures (Fig. 10C). There are fibrils parallel to the
374 cell wall appearing to go through the wall grains similarly to the perithallial cell walls.
375 Interfilament grains are present, as in perithallial cells (Fig. 10B, C). The HCW wall can
376 have two clearly defined morphologies (Fig. 10C). The wall adjacent to the interfilament
377 is narrowest at ~200 nm, has closely spaced organic fibrils and is poorly calcified
378 compared to the inner part of the wall (300-400 nm wide) and appears more like a
379 mineralized membrane. The wider inner part of the cell wall has radial grains but without

380 the well-defined shape of the PCW radial grains. Similar to the perithallial cell walls,
381 there are fibrils appearing to thread through the hypothallial cell wall grains.

382

383 The transitional cells between the hypothallus and perithallus have features from both
384 types present (Fig. 10D). The cell walls can be narrow, <200 nm, poorly mineralized
385 similarly to the outer part of the hypothallial cell wall. Parts of the cell wall resemble the
386 perithallial cell walls, with radial grains and wall width of nearly 1 μm , although along
387 the same wall this changes to ~200 nm wide and a poorly mineralized membrane. The
388 parallel fibrils are also present within the transitional cell walls. Interfilament grains are
389 present comparably to those between hypothallial and perithallial cells.

390

391 **Discussion**

392 *Site temperature, ecology and growth*

393 The site of collection for this specimen (Fig. 1A) is a pavement of coralline encrusted,
394 roughly flat to ovoid shells and pebbles often with dish shapes. Many, such as the
395 specimen employed in this study have a concave surface (due to the original mollusk
396 shape). The benthic surface that we show in figure 1B is likely quite stable with time in
397 the moderate reversing tidal current environment of the site. The conceptacles of *L. leave*,
398 requiring considerable solar energy for construction; all appear on the upper side of the
399 specimen and further assist our determination of orientation. Since the sea ice does not
400 clear the area until late June or early July, solar energy has already peaked, by the time
401 the benthos at 15-17 m receives significant light. Effectively, the growing season is July
402 through November, and with a mean growing season temperature of < 2° C. Based on the

Rob Nash 9/11/17 12:04 PM

Deleted: micron

404 lateral growth rates (5-7 $\mu\text{m}/\text{day}$) found by Adey (1970), a season of lateral growth would
405 provide less than one mm of extension. As we discuss below, the vertical growth in this
406 species is slower than the lateral growth. The layering seen in figure 2B likely represents
407 4-5 years of vertical growth. At 80-100 μm of perithallial addition/year, this relates well
408 to the 100-200 μm /year found with extensive data in the same region for
409 *Clathromorphum compactum* (Adey et al. 2015b).

410

411 Considering that *Leptophytum leave* crusts can be many cm broad and rarely exceed 500
412 μm in thickness, except by overgrowing of earlier crusts, it can be assumed that after
413 initial formation, upwards perithallial growth is either very slow, perhaps limited by the
414 development of conceptacles for which considerable photosynthate must be dedicated. *L.*
415 *leave* is a deep water species (Adey 1966a, b, 1968, 1971) and requires little solar energy
416 to grow and carry out its life cycle; however, as shown by Adey (1970), the rate of
417 hypothallial extension falls with light reduction, and it would be expected that growth on
418 the underside of a shell-encased fragment would be present but less than that on the upper
419 surface.

420

421 *Temperature and magnesium*

422 One of the challenges using samples collected at a single point in time is that the growth
423 history cannot always be precisely tied to previous points in time and temperature. As
424 discussed in the previous section, this crust likely represents 4-5 years of growth. Thus
425 the XRD mol% MgCO_3 is an average for that period. The individual EDS measurement

426 spots cannot be tied to a particular time of year or temperature. However, the annual
427 temperature range is not large, estimated to be ~ 4 °C across the growing season.

428

429 | The XRD Mg content is within the range for average winter and summer Mg contents for
430 *Clathromorphum compactum* collected from Arctic Bay, Kingitok and Quirpon (Halfar et
431 al. 2011, 2013). The EDS-determined average Mg content for each carbonate type had a
432 range of 7.6 mol% MgCO₃, from 9.1 (*K. epilaeve* interfilament) to 16.7 mol% MgCO₃ (*L.*
433 *laeve* upper crust hypothallus). The *L. laeve* upper hypothallus has 84% more Mg than
434 the *K. epilaeve* interfilament. Although the exact time and temperature of formation for
435 each component is not known, the temperature range (~4 °C) alone is highly unlikely to
436 explain the Mg difference. Studies on Mg content in CCA for temperature proxies have
437 used regressions with temperature records to determine a range of responses from 0.266
438 mol % (Williamson et al. 2014), ~1.0 (Halfar et al. 2000; Darrenougue et al. 2013) to
439 1.76 mol% MgCO₃ (Kamenos et al. 2008) per degree celsius of temperature increase.
440 Only the Kamenos et al. (2008) calibration is close to explaining the range here.
441 However, that calibration was for branches of the rhodolith *Lithothamnion glaciale*.
442 Using temperature calibrations for crust CCA in experimental treatments, where
443 temperature was the only condition changed (Diaz-Pulido et al. 2014; Nash et al. 2016), a
444 calibration of 0.33 mol%/°C is obtained. This rate is in agreement with results from
445 Williamson et al. (2014), Chave and Wheeler (1964) and Adey (1965). Using 0.33, a shift
446 of 7.6 mol% equates to 23°C of change, nearly four times greater than the maximum
447 annual range at this site. The magnesium offsets in different parts of the crust are clearly
448 | aligned to anatomical features and not controlled by temperature. [This proposal is](#)

449 [supported by recent results for species of CCA *Phymatolithon* that also demonstrated](#)
450 [anomalously higher Mg in hypothallial cells across four species collected from differing](#)
451 [locations \(Nash and Adey 2017\).](#) Within these offsets there may still be a response to
452 temperature over the seasons, but it was beyond the capacity of this study to investigate
453 seasonal changes. It is noteworthy that the upper crust hypothallus average of 16.7 mol%
454 MgCO₃ is equivalent to new surface crust of tropical *Porolithon onkodes* grown at 30° C
455 (Diaz Pulido et al. 2014).

456

457 *Structural features*

458 There are three main types of calcified structures within the vegetative tissues of
459 *Leptophytum leave* and *Kvaleya epilaeve*: (1) the radial Mg-calcite within the cell walls
460 of the perithallium, (2) the interfilament in both the perithallium and hypothallium and
461 (3) the thin hypothallial cell walls. Each has distinctively different features and
462 magnesium content. The more elongate (and thinner-walled) cells of the hypothallus have
463 been reported for other species of Melobesioideae (Adey 1964, 1965, 1966a). However,
464 this is the first study to show that the internal cell wall Mg-calcite structure and their
465 magnesium content differs from perithallial cell wall. Probably these thinner elongated
466 hypothallial cell walls are a result of relatively rapid growth during lateral extension.
467 There are numerous examples documenting higher Mg in parts of crusts that have grown
468 faster during the warmer seasons (e.g. *Clathromorphum compactum* and *C. nereostratum*
469 by Adey et al. 2013). In this case the [Mg increase is associated with anatomical change,](#)
470 [not temperature.](#) The mechanistic process by which more Mg is incorporated into the
471 HCW and how this relates to growth rate is not known. [The *K. epilaeve* perithallial cells](#)

Rob Nash 9/11/17 1:04 PM

Deleted: re

Rob Nash 9/11/17 1:05 PM

Deleted: is no elevated

474 had lower Mg than the *L. leave* perithallial cells. Cabioch and Giraud (1986) described
475 the perithallial cells as being a later stage of development than epithallial cells.
476 Epithallial cells do not have fully developed rounded cell walls of the perithallial cells
477 (Adey 2015a, b). Although Mg-content of epithallial carbonate is lower than the
478 perithallial values (Diaz-Pulido et al. 2014, Nash et al. 2015, 2016), the lower Mg
479 measured here is not considered a result of different cell type as the *K. epilaeve* cell walls
480 have the radial calcite similarly to the perithallial *L. Leave*, indicating that these are
481 similarly well developed. Considering the time of collection in early summer, it is quite
482 possible that the *K. epilaeve* growth closest to the *L. leave* surface was laid down closer
483 to winter and in cooler temperatures, this being a likely explanation for the lower Mg
484 content.

485

486

487 *Calcification and photosynthesis*

488 The parasitic epiphyte *K. epilaeve* is not known to photosynthesize. The similarity of cell
489 wall and interfilament features to those of the photosynthesizing host, *L. leave*, suggests
490 that the precipitation of the Mg-calcite is not directly driven by photosynthesis as has
491 been suggested for coralline algae (Ries 2010) and demonstrated for calcifying green
492 algae *Halimeda*, (e.g. Adey 1998, Sinutok et al. 2012). Rather, considering also the
493 evidence for continued calcification during the Arctic winter (Halfar et al. 2011, Adey et
494 al. 2013), it seems likely the first control is the provision of the organic substrate that
495 subsequently either becomes calcified or induces calcification. This does not negate the

496 possibility of increased calcification as photosynthetic rates increase (e.g. Borowitzka
497 1981).

498 *Banding and magnesium uptake*

499 The concentric banding of organic fibrils within the perithallial cell wall may offer
500 insight into controls on Mg variation within the cell wall. The dominant visual
501 morphological pattern is the radial Mg-calcite crystals. In contrast, other work indicates
502 the dominant pattern of Mg distribution within the cell may be unrelated to the radial
503 features. Concentric zonations of higher Mg content have been shown, using back scatter
504 electron imaging, in cell walls of tropical *Porolithon onkodes* (Nash et al. 2011).
505 Ragazzola et al. (2016) using NanoSIMs, also showed clear concentric banding of Mg
506 within summer cell walls of *Lithothamnion glaciale*. These published observations
507 together with the results in this study suggest there could be a strong organic control on
508 Mg distribution within the cell, with this being related to the concentric fibrils. Possibly
509 the fibril organics enable higher Mg incorporation than the organics involved in the radial
510 structures. Ragazzola et al. (2016) further documented a decreased prominence of Mg
511 banding in winter cells of *L. glaciale* and for those grown in CO₂ enriched conditions.
512 Results from our study offer an insight as to possible temperature or CO₂-driven
513 ultrastructure changes that may result in decreased Mg content. If the banded fibrils
514 observed in this study are normally similarly present in the *L. glaciale*, then an absence of
515 the Mg bands for their winter and elevated CO₂ treatment suggests that these fibrils could
516 either be absent, or the organic structure or composition has changed and no longer
517 enables elevated Mg.

518

Rob Nash 9/11/17 1:07 PM

Deleted: is interesting from a magnesium perspective.

Rob Nash 9/11/17 1:08 PM

Deleted:

522 *Relevance to Climate Archiving*

523 This study has several implications for climate archiving using corallines. Most
524 importantly, anatomical controls can override temperature influences on Mg composition.
525 We do not suggest current studies are inadequate because the finer scale (submicron)
526 scale variations are not captured. These fine scale variations will not change the general
527 trends or conclusions. Rather, we suggest caution regarding interpretation of data where a
528 change in Mg is visibly associated with a change in cell type as temperature may not be
529 the only possible driver of Mg change. While hypothallial areas can usually be easily
530 excluded from most climate archiving (but see Bougeois et al. 2015), less obvious
531 anatomically different tissues such as the elevated Mg transitional cell walls may not be
532 noticeable at low magnification. This may lead to a false positive result identifying such a
533 region as reflecting a time of higher temperature. As well as these tissue-scale differences,
534 the cellular scale differences may also need to be considered. Any seasonal change in
535 relative proportion of CW to IF can shift the [Mg] in absence of any temperature-
536 influenced change. For example if CW = 10 mol% MgCO₃ and IF = 8 mol% MgCO₃,
537 and crust changes from 90:10 CW:IF to 50:50 this would equate to a change in of 9.8 to 9
538 mol% for measurements of bulk crust (i.e. spot sizes larger than the cell size, or smaller
539 spot sizes averaged without reference to their anatomical placement). This change
540 equates to a 2-3 degrees using a temperature calibration of 0.33 mol% MgCO₃ °C. Should
541 the difference in cell wall and interfilament mol% MgCO₃ be larger, then the total
542 average will change more substantially. Furthermore, the bulk magnesium results for
543 different CCA species with differing proportions of cell wall:interfilament from the same
544 temperature environments will have a range of non-temperature related Mg content that is

545 controlled by the cell wall:interfilament. This change in structure, if seasonally correlated,
546 will be indirectly related to temperature, but there may be other influences such as light.

547 For example, CCA continue to grow in darkness using stored photosynthates, after ice
548 sheets have formed above (Halfar et al. 2013), however, it is not known if a switch to
549 using stored energy results in any anatomical changes. If there were changes, these would
550 only be indirectly related to temperature. More recently Sletten et al. (2017) found
551 anatomical changes (banding) in *Lithothamnion* rhodoliths were unrelated to temperature
552 and proposed these were driven by differences in light exposure. Thus, the best CCA
553 temperature climate archives, as compared to seasonal archives, are likely to be those
554 with the least seasonally varying ultrastructure changes.

555

556 Understanding the combined contribution of anatomical and temperature changes to
557 measured magnesium may help explain the variation of Mg-temperature calibrations in
558 the published literature. Typically it is the rhodoliths that show the highest response of
559 Mg to temperature, e.g. *Lithothamnion glaciale* at 1- 1.76 mol% MgCO₃ (Halfar et al.
560 2000; Kamenos et al. 2008) per degree celsius of temperature increase compared to
561 *Clathromorphum compactum* at 0.7 mol% MgCO₃ (Halfar et al. 2010). The *L. glaciale*
562 has distinct seasonal changes shifting to a clear band of elongated cells during summer.

563 The rhodolith summer cells have similarities in appearance to the hypothallial cells in this
564 study. Possibly the higher measured Mg in the long cells of the rhodolith is a result in
565 part of a switch towards a more perithallial style cell and may not be entirely temperature
566 related. This proposition is supported by Sletten et al. (2017) who found a switch to

567 | [elongated cells with higher Mg that was unrelated to seasonality](#). In contrast, anatomical
568 changes in *C. compactum* (Adey et al. 2013) are not so extreme.

569

570 *Suggestions for improving analytical methods*

571 | Our work is ongoing in this area of research and as more species and ultrastructures are
572 studied we expect to be able to provide more detailed guidance on utilizing Mg from
573 CCA for climate proxies. However, in the interim, there are several steps that could be
574 incorporated into routine analyses to improve the accuracy of Mg climate proxies. Firstly,
575 it should become a routine part of analyses that the ultrastructure is assessed to determine
576 if the ratio of cell wall to interfilament carbonate changes regularly with seasons. Second,
577 | when possible as well as the larger spot sizes used in sampling transects, e.g. 10-20 [µms](#),
578 make discrete spot analyses using the smallest reliable interaction volume possible to
579 determine indicative Mg offsets between the cell wall and interfilament so that this can be
580 adjusted for if necessary, in the final interpretation. Third, ensure that hypothallial growth
581 is not included in sampling transects. Usually the basal hypothallus is easily avoided, but
582 secondary hypothallus and transitional cells may be harder to avoid without careful SEM
583 analysis.

584

585 **Conclusion**

586 It appears that within these CCA, there is a strong control on the uptake of Mg in relation
587 to the different anatomical components. This is in contrast to the suggestion by Ries
588 (2010), based on Mg:Ca in seawater manipulation experiments, that corallines exert little
589 | or no control over their Mg uptake other than to specify the polymorph. [Recent work](#)

Rob Nash 9/11/17 12:04 PM

Deleted: micron

591 indicates that the interfilament and perithallial carbonate react similarly to temperature,
592 but the responsive hypothallial carbonate is inconclusive (Nash and Adey 2017). It would
593 be interesting to identify if each of interfilament, perithallial and hypothallial cell walls
594 reacted similarly to changes in seawater Mg:Ca, or if there were differences in anatomical
595 controls. Crucially, it is necessary to keep in mind the biological controls on Mg uptake
596 when using CCA Mg changes as a climate proxy.

597

598 While the focus of this study has been the distribution of Mg with different anatomical
599 features, the high-magnification images are the first to show the cellular-scale organic
600 structures together with the carbonate components. The orientation of the crystals in the
601 interfilament and the cell walls are in agreement with lower-magnification SEM studies
602 on a range of algal species (Cabioch and Giraud 1986, Adey et al. 2013). The
603 combination of gentle etching and high-magnification SEM has revealed previously
604 unknown features such as the fibrils threading through the radial Mg-calcite (Fig. 7C).
605 Further, showing that the Mg content varies with anatomical features suggests that the
606 calcification may be a different process, or have different controls, for each carbonate
607 type. This adds an extra level of complexity when considering how environmental
608 changes, such as increasing temperature, may impact on the capacity of the CCA to
609 continue their important substrate provision ecological role.

610

611 **Acknowledgments**

612 Thanks to the Centre for Advanced Microscopy at the Australian National University and
613 the Mineral Sciences department at the Smithsonian Institution for assistance with SEM-
614 EDS.

615

616 **References**

617 Adey, W. 1964. The Genus *Phymatolithon* in the Gulf of Maine. *Hydrobiologia*
618 24:377-420.

619 Adey, W. 1965. The Genus *Clathromorphum* in the Gulf of Maine. *Hydrobiologia*
620 26:539-573.

621 Adey, W. 1966a. The Genera *Lithothamnium*, *Leptophytum* (nov. gen.) and
622 *Phymatolithon* in the Gulf of Maine. *Hydrobiologia* 28:321-368.

623 Adey, W. 1966b. The Genus *Pseudolithophyllum* in the Gulf of Maine.
624 *Hydrobiologia* 27:479-597.

625 Adey, W. 1966c. The Distribution of Saxicolous Crustose Corallines in the
626 Northwestern North Atlantic. *J. Phycol.* 2:49-54.

627 Adey, W. 1970. The Effects of Light and Temperature on Growth Rates in
628 Boreal-Subarctic Crustose Corallines. *J. Phycol.* 6:269-276.

629 Adey, W. 1973. Temperature Control of Reproduction and Productivity in a
630 Subarctic Coralline Alga. *Phycologia* 12:111-118.

631 Adey, W. 1978a. Coral Reef Morphogenesis: A Multidimensional Model.
632 *Science* 202:831-837.

633 Adey, W. 1978b. Algal Ridges of the Caribbean Sea and West Indies. *Phycologia*
634 17:361-367.

635 Adey, W. 1998. Coral Reefs: algal structured and mediated ecosystems in shallow,
636 turbulent alkaline seas. *J. Phycol.* 34:393-406.

637 Adey, W. & D. McKibbin. 1970. Studies of the Maerl Species of the Ria de Vigo.
638 *Bot. Mar.* 8:100-106.

639 Adey, W. & C. Sperapani. 1971. The Biology of *Kvaleya epilaeve*, A New
640 Parasitic Genus and Species of Corallinaceae. *Phycologia* 10:29-42.

641 Adey, W., T. Masaki & H. Akioka. 1974. *Ezo epiyessoense*, A New Parasitic Genus and
642 species of Corallinaceae. *Phycologia* 13:329-344.

643 Adey, W. & J. M. Vassar. 1975. Colonization, Succession and Growth Rates of
644 Caribbean Crustose Corallines. *Phycologia* 14:55-69.

645 Adey, W., Y. Chamberlain, & L. Irvine. 2005. A SEM-Based Analysis of the
646 Morphology, reproduction and ecology of *Lithothamnion tophiforme* Unger
647 (Corallinales, Rhodophyta), an Arctic coralline. *J. Phycol.* 41:1010-1024.

648 Adey, W., Lindstrom, S., Hommersand M. & Muller, K. 2008. The biogeographic origin
649 of Arctic endemic seaweeds: A thermogeographic view. *J. Phycol.* 44:1384-1394.

650 Adey, W., Halfar, J. & Williams, B. 2013. The coralline genus *Clathromorphum* Foslie
651 emend Adey; biological, physiological and ecological factors controlling
652 carbonate production in an Arctic/Subarctic climate archive. *Smithsonian*
653 *Contributions to the Marine Sciences* 40:1-83.

654 Adey, W., Hernandez-Kantun, J. J., Johnson, G. & Gabrielson, P. 2015a. DNA
655 sequencing, anatomy and calcification patterns support a monophyletic, Subarctic,
656 carbonate reef-forming *Clathromorphum* (Hapalidiaceae, Corallinales,
657 Rhodophyta). *J. Phycol.* 51:189-203.

658 Adey, W., Halfar, J., Humphreys, A. Belanger, D., Gagnon, P. & Fox, M. 2015b.
659 Subarctic rhodolith beds promote longevity of crustose coralline algal buildups
660 and their climate archiving potential. *Palaios* 30:281-293.

661 Amado-Filho, G., Moura, R., Bastos, A., Salgado, L., Sumida, P., Guth, A., Francini-
662 Filho, R., Pereira-Filho, G., Abrantes, D., Brasileiro, P., Bahia, R., Leal, R.,
663 Kaufman, L., Kleypas, J., Farina, M. & Thompson, F. 2012. Rhodolith Beds are
664 major CaCO₃ bio-factories in the Tropical South West Atlantic. *Plos One* 7
665 (4):e35171.

666 Bahia, R., Abrantes, D., Brasileiro, P., Pereira-Filho, G. & Amado-Filho, G. 2010.
667 Rhodolith bed structure along a depth gradient on the northern coast of Bahia
668 State, Brazil. *Brazilian J. Oceanography* 58:323–337.

669 Barnes, D. J., & Lough, J. M. 1993. On the nature and causes of density banding in
670 massive coral skeletons. *J. Exp. Mar. Biol. Ecol.* 167:91-108.

671 Bentov, S., & Erez, J. 2005. Novel observations on biomineralization processes in
672 foraminifera and implications for Mg/Ca ratio in the shells. *Geology* 33:841-844.

673 Borowitzka, M. A. 1981. Photosynthesis and Calcification in the Articulated Coralline
674 Red Algae *Amphiroa anceps* and *A. foliacea*. *Mar. Biol.* 62:17-23.

675 Bougeois, L., Williams, B., Halfar, J., Konar, B., Adey, W., Kronz, A. & Wortmann, U.G.
676 2015. Does the coralline alga *Leptophytum fœcundum* (Kjellman) capture
677 paleoenvironmental variability in the Arctic Ocean? *Arctic, Antarctic, and Alpine*
678 *Research* 47:375-387.

679 | Chave, K. & B. Wheeler. 1965. Mineralogical changes during growth in the red alga
680 | *Clathromorphum compactum*. *Science* 147:621.

681 [Cox, T. E., M. Nash, F. Gazeau, M. Déniel, E. Legrand, S. Alliouane, P. Mahacek, A. Le](#)
682 [Fur, J-P. Gattuso, & S. Martin. 2017. Effects of in situ CO2 enrichment on](#)
683 [Posidonia oceanica epiphytic community composition and mineralogy. *Mar.*](#)
684 [Biol. 164:103.](#)

685 Darrenougue, N., De Deckker, P., Payri, C., Eggins, S., & Fallon, S. 2013. Growth and
686 chronology of the rhodolith-forming, coralline red alga *Sporolithon*
687 *durum*. *Marine Ecology Progress Series* 474:105-119.

688 [Diaz-Pulido, G., Nash, M.C., Anthony, K.R., Bender, D., Opdyke, B.N., Reyes-Nivia, C.](#)
689 [& Troitzsch, U., 2014. Greenhouse conditions induce mineralogical changes and](#)
690 [dolomite accumulation in coralline algae on tropical reefs. *Nature*](#)
691 [communications, 5.](#)

692

693 Esau, K. 1953. *Plant Anatomy*. John Wiley and Sons. New York. 735 pp.

694 Nash, M. C., Opdyke, B. N., Troitzsch, U., Russell, B. D., Adey, W. H., Kato, A., Diaz-
695 Pulido G., et al. 2013. Dolomite-rich coralline algae in reefs resist dissolution in
696 acidified conditions. *Nat. Clim. Change* 3:268-272.

697 Halfar, J., Zack, T., Kronz, A., & Zachos, J. C. 2000. Growth and high-resolution
698 paleoenvironmental signals of rhodoliths (coralline red algae)- A new biogenic
699 archive. *J. Geophysical Research* 105:22-107.

700 Gamboa, G., Halfar, J., Hetzinger, S., Adey, W., Zack, T., B. Kunz, B., & Jacob, D. 2010.
701 Mg/Ca ratios in coralline algae as proxies for NW Atlantic temperature variations.
702 *J. Geophysical Research-Oceans* 115:1-12.

Rob Nash 9/11/17 11:51 AM
Formatted: Font:(Default) Times New Roman, 12 pt

Rob Nash 9/11/17 11:51 AM
Formatted: Font:English (AUS)

703 Halfar, J., Hetzinger, S., Adey, W., Zack, T., Gamboa, G., Kunz, B., Williams, B., Jacob,
704 D. 2010. Coralline algal growth increment widths archive North Atlantic climate
705 variability. *Palaeogeography, Palaeoclimatology, Palaeoecology* 302:71-80
706 Halfar, J., Adey, W., Kronz, A., Edinger, E., & W. Fitzhugh, W. 2013. Unprecedented
707 sea-ice decline archived by novel multi-century annual-resolution algal proxy.
708 *PNAS* 110: 197837-19741.
709 Harvey, A. S., Harvey, R. M., & Merton, E. 2016. The distribution, significance and
710 vulnerability of Australian rhodolith beds: a review. *Marine and Freshwater*
711 *Research* doi.org/10.1071/MF15434.
712 Hetzinger, S., Halfar, J., Kronz, A., Steneck, R.S., Adey, W., Lebednik, P. A. & Schone,
713 B. R. 2009. High-Resolution Mg/Ca Ratios in a coralline Red Alga As a Proxy
714 for Bering Sea Temperature Variations from 1902-1967. *Palaios* 24:406-412.
715 Kamenos, N., Cusack, M., & Moore, P. G. 2008. Coralline Algae Are Global
716 Paleothermometers with Bi-Weekly Resolution. *Geochimica et Cosmochimica*
717 *Acta* 72:771–779.
718 Kamenos, N. A., & Law, A. 2010. Temperature controls on coralline algal skeletal
719 growth. *J. Phycol.* 46:331-335.
720 Krayesky-Self, S., Richards, J., Rahmatian M., & Fredericq, S. 2016. Aragonite infill in
721 overgrown conceptacles of coralline Lithothamnion spp (Hapalidaceae,
722 Hapalidiales, Rhodophyta): new insights in biomineralization and
723 phylominerology. *J. Phycol.* 52:161-173.

724 Martin, C. S., Giannoulaki, M., De Leo, F., Scardi, M., Salomidi, M., Knittweis, L., Pace,
725 M. L. et al. 2014. Coralligenous and maërl habitats: predictive modelling to
726 identify their spatial distributions across the Mediterranean Sea. *Sci. Rep.* 4.
727 McCoy, S. J., & Kamenos, N. A. 2015. Coralline algae (Rhodophyta) in a changing
728 world: integrating ecological, physiological, and geochemical responses to global
729 change. *J. Phycol.* 51:6-24.
730 [Nash, M.C. & Adey, W., 2017. Multiple phases of mg-calcite in crustose coralline algae](#)
731 [suggest caution for temperature proxy and ocean acidification assessment: lessons](#)
732 [from the ultrastructure and biomineralisation in Phymatolithon \(Rhodophyta,](#)
733 [Corallinales\). *J. Phycol.* In press. 10.1111/jpy.12559](#)
734 Nash, M. C., Troitzsch, U., Opdyke, B., Trafford, J., Russell, B., & Kline, D. 2011. First
735 discovery of dolomite and magnesite in living coralline algae and its
736 geobiological implications. *Biogeosciences*. 8, 3331-3340.
737 Nash, M. C., Opdyke, B. N., Wu, Z., Xu, H. & Trafford J. M. 2013. Simple X-ray
738 diffraction techniques to identify Mg calcite, dolomite, and magnesite in tropical
739 coralline algae and assess peak asymmetry. *J. Sed. Res.* 83:1085-1099.
740 Nash, M. C., Uthicke, S., Negri, A.P., & Cantin, N. E. 2015. Ocean acidification does not
741 affect magnesium composition or dolomite formation in living crustose coralline
742 algae, *Porolithon onkodes* in an experimental system. *Biogeosciences* 12:5247-
743 5260.
744 Nash M.C., Martin S., Gattuso J-P. 2016. Mineralogical response of the Mediterranean
745 crustose coralline alga *Lithophyllum cabiochae* to near-future ocean acidification
746 and warming. *Biogeosciences Discussions* doi:10.5194/bg-2016-160.

747 [Ragazzola, F., Foster, L. C., Jones, C. J., Scott, T. B., Fietzke, J., Kilburn, M. R., &](#)
748 [Schmidt, D. N. 2016. Impact of high CO₂ on the geochemistry of the coralline](#)
749 [algae *Lithothamnion glaciale*. *Scientific reports*, 6, 20572.](#)

750 Ries, J. 2010. Review: Geological and Experimental Evidence for Secular Variation in
751 Seawater Mg/Ca (Calcite-Aragonite Seas) and Its Effects on Marine Biological
752 Calcification. *Biogeosciences*, 7:2795–2849.

753 [Sletten, H. R., Andrus, C. F. T., Guzmán, H. M., & Halfar, J. 2017. Re-evaluation of](#)
754 [using rhodolith growth patterns for paleoenvironmental reconstruction: An](#)
755 [example from the Gulf of Panama. *Palaeogeography, Palaeoclimatology,*](#)
756 [Palaeoecology 465:264-277.](#)

757 Sinutok, S., Hill, R., Doblin, M. A., Kühl, M., & Ralph, P. J. 2012. Microenvironmental
758 changes support evidence of photosynthesis and calcification inhibition in
759 *Halimeda* under ocean acidification and warming. *Coral Reefs* 31:1201-1213.

760 Sherman, C.E., Fletcher, C., Rubin, K., Simmons, K. & Adey, W. 2014. Sea-level and
761 reef accretion history of Marine Oxygen Isotope Stage 7 and late stage 5 based on
762 age and facies of submerged late Pleistocene reefs, Oahu, Hawaii. *Quaternary Res.*
763 81:138-150.

764 [Sletten, H.R., Andrus, C.F.T., Guzmán, H.M. & Halfar, J., 2017. Re-evaluation of using](#)
765 [rhodolith growth patterns for paleoenvironmental reconstruction: An example](#)
766 [from the Gulf of Panama. *Palaeogeography, Palaeoclimatology,*](#)
767 [Palaeoecology, 465:264-277.](#)

768

769 [Vásquez-Elizondo, R.M. and Enríquez, S., 2016. Coralline algal physiology is more](#)
 770 [adversely affected by elevated temperature than reduced pH. *Scientific reports*, 6,](#)
 771 [p.19030.](#)

772 Wanamaker, A., Kreutz, K., Schone, B., Pettigrew, N., Borns, H., Introne, D., Belknap,
 773 D., Maasch, K. & Feindel, S. 2008. Coupled North Atlantic slope water forcing
 774 on Gulf of Maine temperatures over the past millennium. *Climate Dynamics*
 775 31:183-194.

776 Williamson, C. J., Najorka, J., Perkins, R., M. L. Yallop, M. L. & Brodie, J. 2014.
 777 Skeletal mineralogy of geniculate corallines: providing context for climate change
 778 and ocean acidification research. *Marine ecology progress series* 513:71-84.

779

780 **Tables**

	<i>K. epilaeve</i>		<i>L. laeve</i>					
	IF	CW	CW Under	CW Upper	CW comb.	Under Hyp.	Upper transit.	Upper Hyp.
mol% MgCO₃	9.1%	10.1%	11.2%	12.9%	12.2%	12.3%	15.6%	16.7%
St. Dev.	1.0%	1.2%	1.2%	2.5%	2.2%	0.7%	1.7%	1.7%
Mg/Ca	0.100	0.113	0.126	0.149	0.138	0.140	0.185	0.200

781 **Table 1: SEM-EDS results. Conversion of mol% to Mg/Ca is included.**

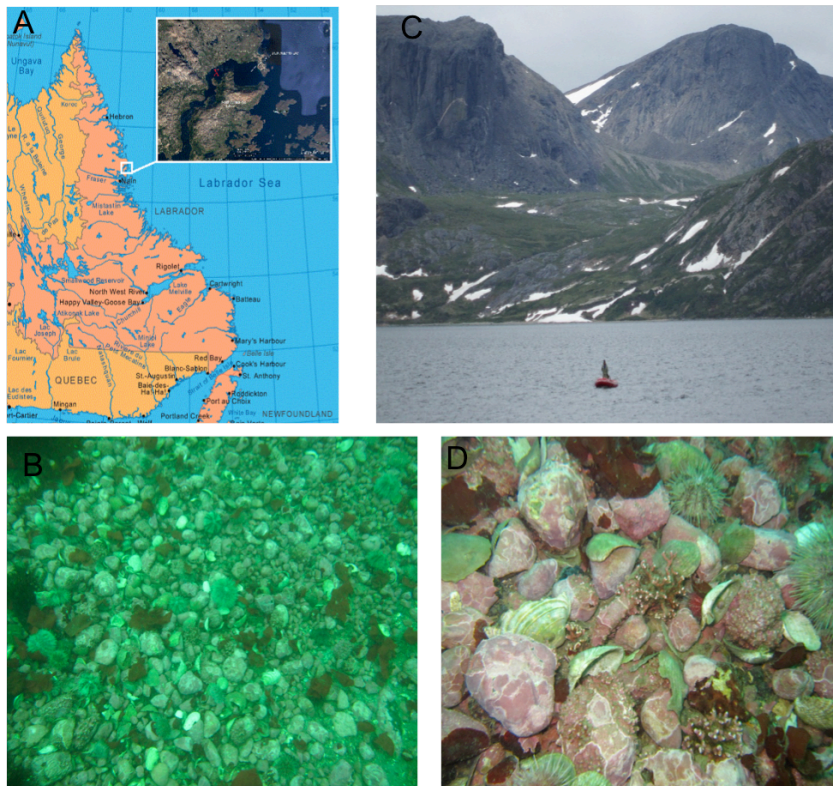
	Average mol% and n	<i>K. epilaeve</i> IF	<i>K. epilaeve</i> CW	<i>L. laeve</i> under CW	<i>L. laeve</i> upper CW	<i>L. laeve</i> CW both	<i>L. laeve</i> under Hyp.	<i>L. laeve</i> upper Hyp.
<i>K. epilaeve</i> IF	9.1 % n=9							
<i>K. epilaeve</i> CW	10.1% n=8	0.069						
<i>L. laeve</i> under CW	11.2% n=8		0.129					
<i>L. laeve</i> upper CW	12.9% n=9		0.012	0.112				

<i>L. leave CW both</i>	12.2% n=17		0.024					
<i>L. laeve under Hyp.</i>	12.3% n=8			0.052	0.470	0.914		
<i>L. laeve upper Hyp.</i>	16.7% n=8					<0.001	<0.001	
<i>L. laeve upper trans.</i>	15.6% n=8					<0.001	<0.001	0.259

782 Table 2: T-test *p* values for 15 kV spot EDS.

783

784 **Figures**

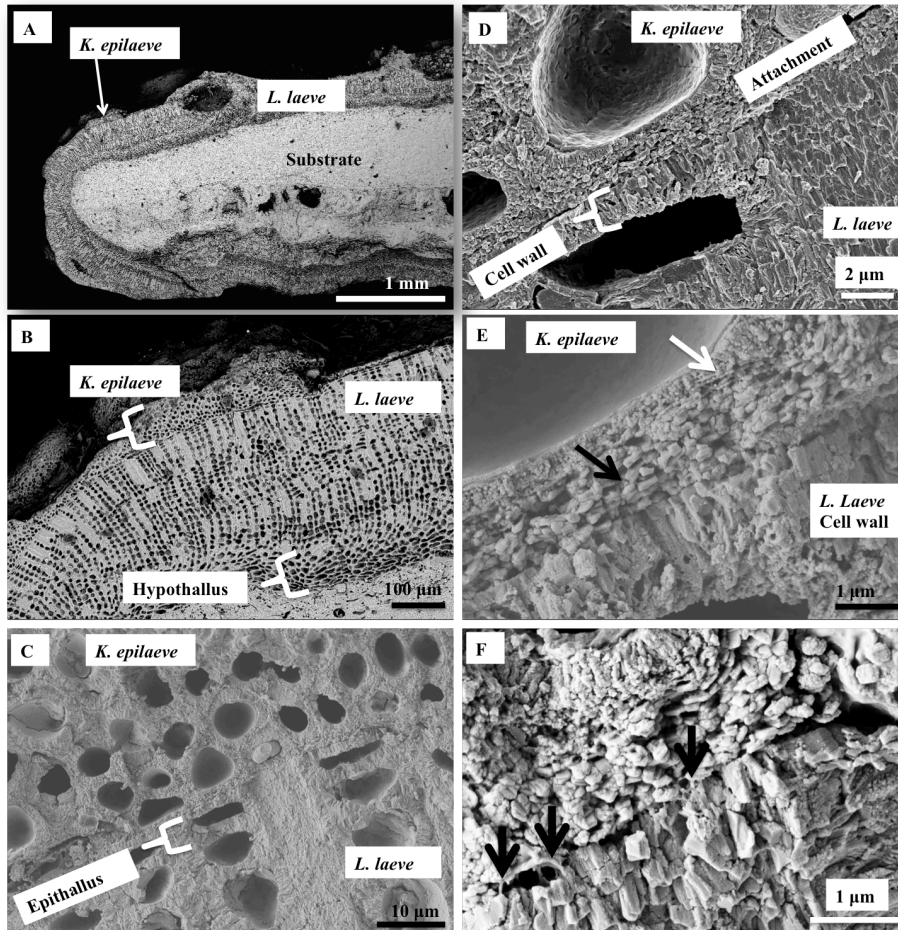


785

786 Figure 1: A. Port Manvers Bay Station, Labrador. B. Pebble/shell bottom with occasional rhodoliths at 15-

787 17 m. Coralline covered pebbles range from about 5-10 cm diameter. C. Collecting site in western Port

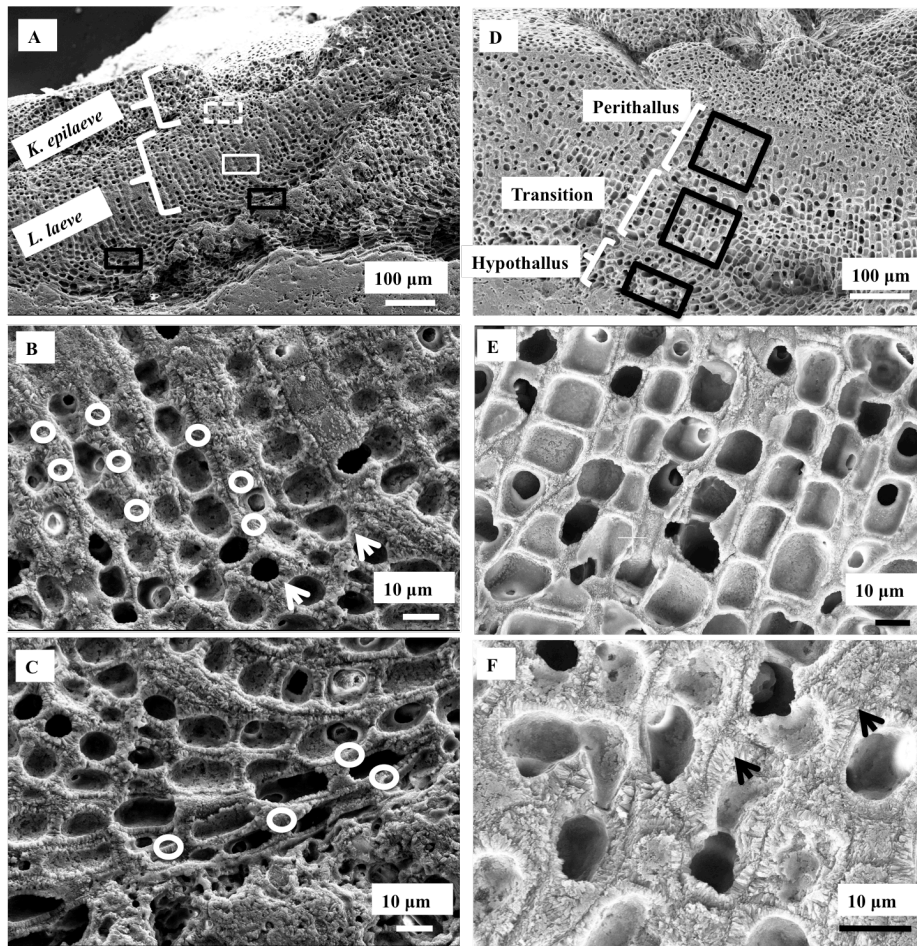
788 Manvers Bay. D. Close-up of bottom shown in figure 1C.



789

790 Figure 2: Overview of *K. epilaeve* on *L. laeve*. **A.** Overview (BSE). *L. laeve* has been partly overgrown by
 791 *K. epilaeve*. **B.** Closer up (BSE) *K. epilaeve* has a very thin perithallium with thicker buildup for its
 792 conceptacle. **C.** Close up (SE) and **D** showing attachment zone of *K. epilaeve* hypothallus on the epithallus
 793 of the *L. laeve*. **E.** (SE) The cell wall in the *L. laeve* is roughly radial whereas the *K. epilaeve* cell wall does
 794 not appear properly mineralized with nm-scale beads of Mg-calcite along what appears to be organic fibrils
 795 (white arrow). The *K. epilaeve* Mg-calcite layer at the attachment zone has coarse angular grains roughly
 796 parallel to the *L. laeve* surface (black arrow). **F.** (SE) Organic fibrils are visible (black arrows) between the
 797 base of the *K. epilaeve* and the surface of the *L. laeve* suggesting this is the attachment mechanism.

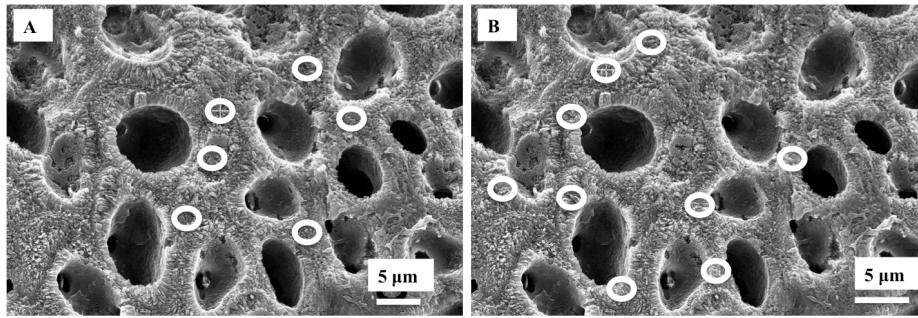
Rob Nash 9/11/17 1:49 PM
 Deleted: meristem



799

800 | Figure 3: Overview of *L. laeve* and *K. epilaeve* and EDS sites (white circles) in *L. laeve*. A-C. Sites on the
 801 | underside of the pebble. D-F. Sites on the upper side of the pebble. A. White dashed box- cell wall and
 802 | interfilament in *K. epilaeve*. White box- perithallial cell wall *L. laeve*. Black box- hypothallus *L. laeve*. B.
 803 | EDS sites for cell wall measurements of *L. laeve*. Circle size indicates approximate area of measurement (3
 804 | μm s). Cell wall radial Mg-calcite (arrowheads). C. EDS sites for hypothallus (right box in A). D. EDS sites
 805 | on sample upper side for *L. laeve*. E. *L. laeve*. F. *L. laeve*. Cell walls in upper side are visually comparable
 806 | to cell walls in underside with radial Mg-calcite (arrowheads) in cell walls and minimal interfilament.

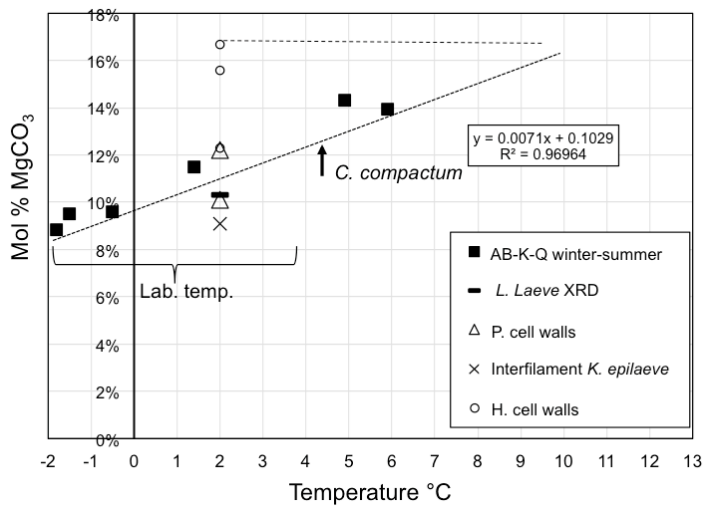
Rob Nash 9/11/17 12:04 PM
 Deleted: micron



808

809 Figure 4: Detail of EDS sites in *K. epilaeve* (dashed white box in Fig. 2A) **A.** EDS sites (white circles) for
 810 interfilament. **B.** EDS sites for cell wall.

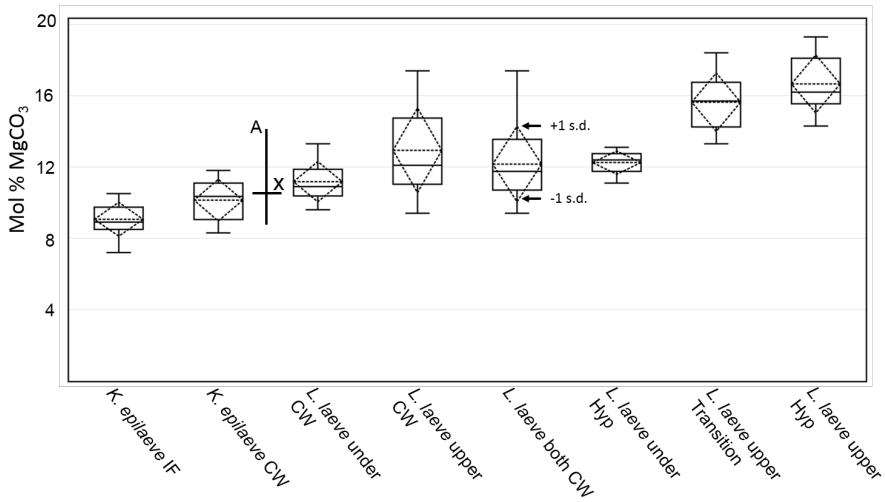
811



812

813 Figure 5: *L. Laeve* and *K. epilaeve* Mg content relative to *Clathromorphum compactum* from Arctic Bay,
 814 Kingitok and Quirpon (Halfar et al. 2010, 2013). Lab – Labrador sea. Heavy dashed line- best fit for *C.*
 815 *compactum*. Light dashed line- indicates the temperature equivalent on the *C. compactum* line for the *L.*
 816 *laeve* hypothallial Mg-content.

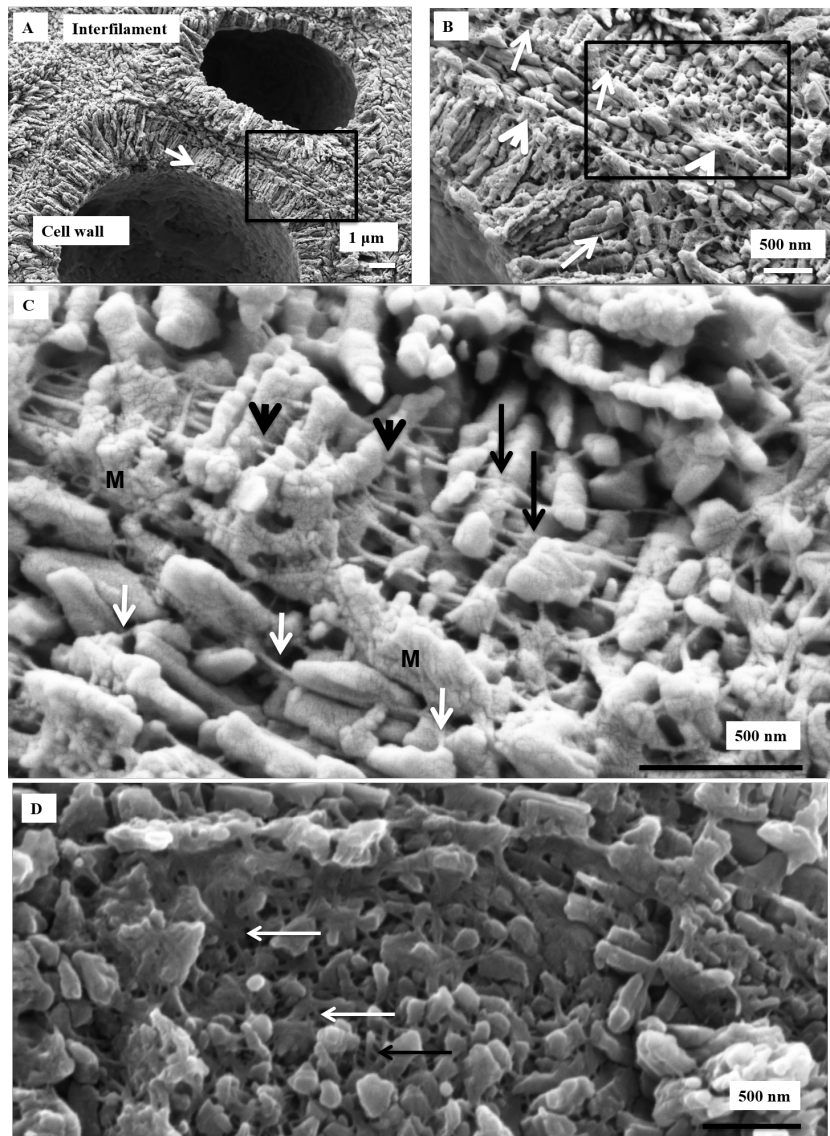
817



818

819 Figure 6: Box plot of EDS mol% MgCO₃ results. Box represents the 2nd and 3rd quartiles. The lower and
 820 upper bars are the minimum and maximum values (excluding an outlier for *L. laeve* under cell wall). The
 821 solid middle line within the box is the median value and the dash middle line the average. The dashed
 822 diamond box represents one standard deviation. The drawn-on cross represents the XRD mol% (X) and the
 823 seasonal range (A) of mol% for the Arctic Bay – Kingitok – Quirpon dataset in figure 5.

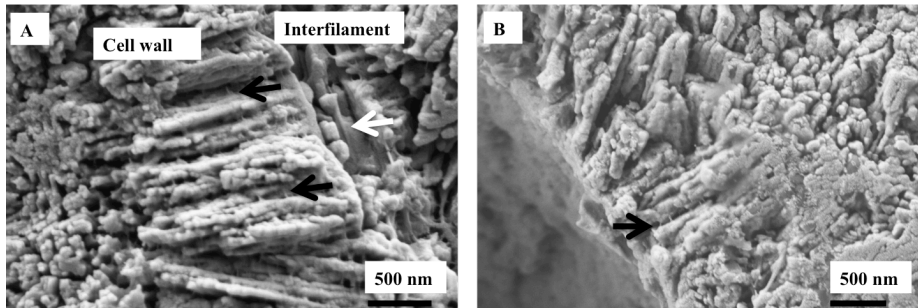
824



825

826 Figure 7: *K. epilaeve* cell wall structure. Crust polished and cleaned for 2 minutes. **A.** Cell walls have radial
 827 Mg-calcite whereas the interfilament grains are orientated either parallel to the filament axis or randomly
 828 within the corner junctions. Within the radial cell walls a secondary concentric banding pattern is visible
 829 (white arrow). Black box enlarged in **B.** **B.** Organic fibrils, ~10nm wide, run parallel to cell wall edges

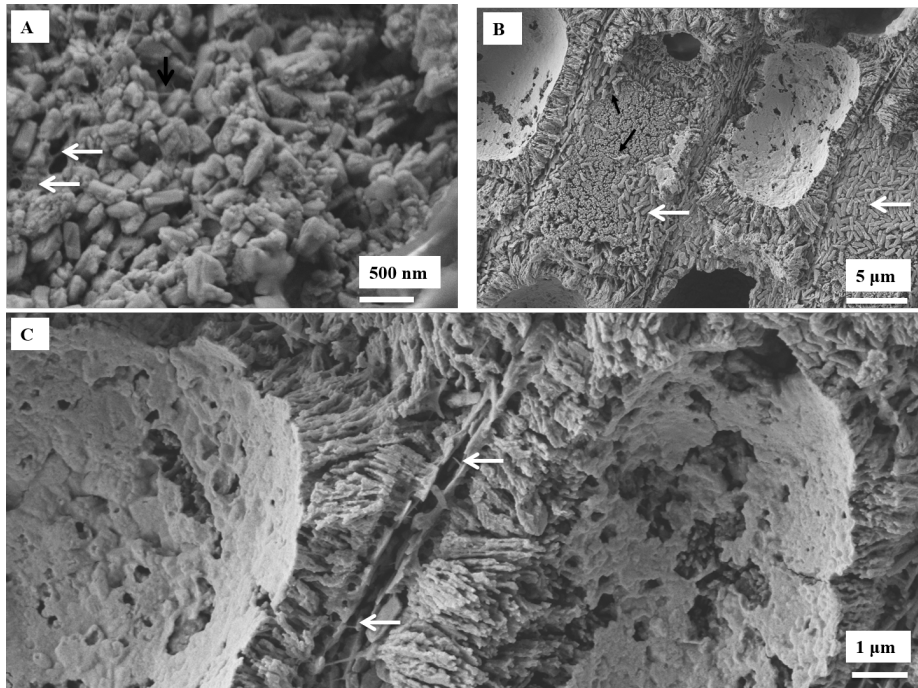
830 (black arrows). Fibrils are concentrated along the outer of the cell wall (white arrows). Black box enlarged
831 in C. C. The cell wall fibrils appear to string through the centre of the radial grains (black arrowheads),
832 Other fibrils drape over the grains (black arrows). Fibrils are present in the interfilament (white arrows). M
833 – mineralized membrane. D. Plan view of cell wall grains. Organic fibrils form a dense mesh (white
834 arrows).
835



836
837 Figure 8: *L. laeve* cell wall structure. A. Cleaned for 2 minutes. Cell wall radial crystals are 1.5 μm length
838 cylindrical grains. Fibrils are present (black arrows) but not as easy to see as in the *K. epilaeve*.
839 Interfilament grains parallel to cell wall with organic fibrils (white arrows) also running parallel to cell wall.
840 B. Etched for 20 minutes. Fibrils appear similarly as in the *K. epilaeve* with the fence post-wire structure
841 (black arrows).
842

Rob Nash 9/11/17 12:04 PM

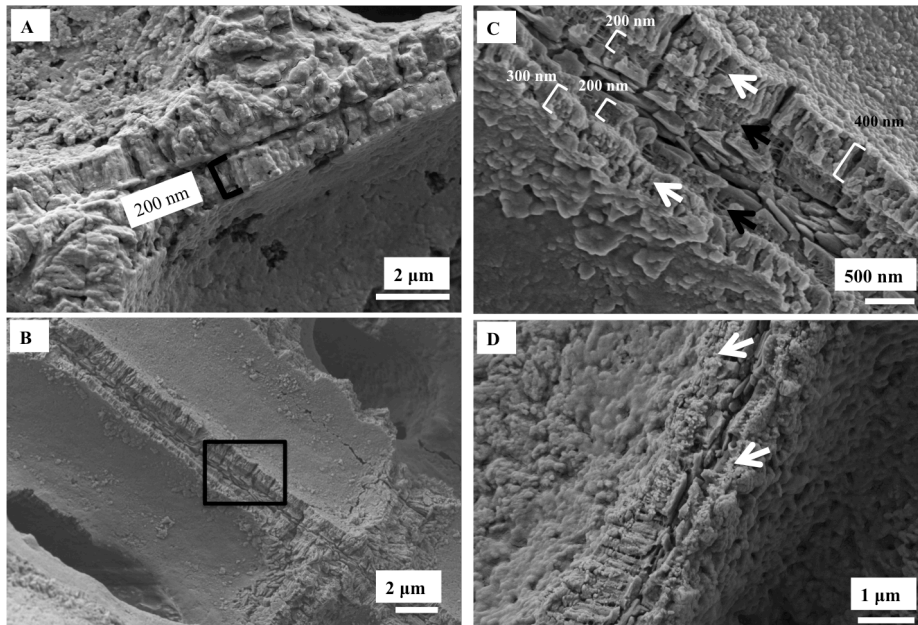
Deleted: micron



844

845 Figure 9: Interfilament structures in *K. epilaeve* (A) and *L. laeve* (B, C). A. *K. epilaeve* etched for 20
 846 minutes. Fibrils (black arrow) and porous membrane (white arrows). B. *L. Laeve* etched for 20 minutes.
 847 Interfilament grains are flattened against the external sides of the cell wall (white arrows) attached by
 848 fibrils (black arrows). C. Fibrils visible stretched across the space between cell walls with 2 layers of
 849 interfilament grains (white arrows).

850



851

852 Figure 10: Hypothallus and transitional cells in *L. leave*. Cleaned 2 minutes. **A.** Hypothallus underside.

853 Organic film covering wall structures. Walls ~200 nm wide, roughly radial structure within cell wall. **B.**

854 Cleaned 2 minutes, hypothallus in upper crust. Roughly radial structure within cell walls. Black box

855 enlarged in C. **C.** The wall adjacent to the interfilament is narrowest at ~200 nm, has closely spaced organic

856 fibrils (black arrows) and is poorly calcified compared to the inner part of the wall (300-400 nm wide)

857 where radial grains are present. There are fibrils parallel to the cell wall appearing to go through the wall

858 grains similarly to the perithallial cell walls (white arrows). **D.** Transitional cell wall. The calcification in

859 the lower of the left side wall is comparable to the perithallial cell wall with radial grains. The right side

860 wall and upper part of the left side (white arrows) are poorly calcified and appear as a calcified membrane

861 rather than a properly developed cell wall.

862